Catalytic degradation of "trinitrogen" by Fe-Ce-SiO2 aerogel@TiO2

Jie Li
East China University of Science and Technology
Yuxiang Yang (yxyang@ecust.edu.cn)
East China University of Science and Technology https://orcid.org/0000-0003-1836-1341
zhiyong Han
Chengdu University of Technology
yan Huang
East China University of Science and Technology
hongming Yuan
Jilin University
chaoying Ni
University of Delaware

Research Article

Keywords: "Three Nitrogen" degradation, Fenton oxidation, Photocatalysis

Posted Date: October 31st, 2022

DOI: https://doi.org/10.21203/rs.3.rs-2027823/v1

Catalytic degradation of "trinitrogen" by Fe-Ce-SiO_2 aerogel@TiO_2

Jie Li[a], Yuxiang Yang[a,c*], Zhiyong Han[b], Yan Huang[a], Hongming Yuan[d], Chaoying Ni[c]

[a]*School of Chemistry and Molecular Engineering, East China University of Science & Technology, Shanghai 200237, China*

[b]*State Key Laboratory of Geohazard Prevention and Geoenvironment Protection (Chengdu University of Technology), Chengdu 610059, P.R.China*

[c]*Department of Materials Science and Engineering, University of Delaware, Newark, Delaware 19716, United States*

[d]*State Key Laboratory of Inorganic Synthesis and Preparative Chemistry, Jilin University, Changchun 130012, China*

**Corresponding author:* yxyang@ecust.edu.cn, cni@udel.edu

Abstract

The "Three nitrogens" [Ammonia nitrogen (NH_4^+ -N), Nitrate nitrogen (NO_3^- -N) and Nitrite nitrogen (NO_2^- -N)] from industrial or domestic wastewater can lead to eutrophication of water bodies, ammonia The conversion of nitrogen into nitrate nitrogen will cause high nitrogen and oxygen demand (NOD), which will also lead to methemoglobinemia, and the high content of nitrite in the water body will increase the risk of cancer. In this paper, SiO_2 aerogel is used as a carrier to synthesize Fe-Ce bimetal-doped composite materials (Fe-Ce/SiO_2 and Fe-Ce-SiO_2/TiO_2) for the adsorption and degradation of "three nitrogens". The effect of metal Fenton reagent (Fe-Ce/SiO_2) Fenton catalysis and photo-Fenton cooperative catalysis (Fe-Ce-SiO_2/TiO_2) on the degradation efficiency of "three nitrogens".

SiO_2/TiO_2 was prepared by dipping method, and Fe and Ce bimetals were loaded on the surface of SiO_2/TiO_2 material, and the effect of photo-Fenton oxidation on the degradation rate of "three nitrogen" under different materials was explored. The results showed that: when the dosage of catalyst was 0.01 g, pH value was 11.0, and the concentration of H_2O_2 was 80 mmol/L, the photocatalytic efficiency was the best, and the degradation efficiency of "three nitrogen" remained above 70%.

Keywords: "Three Nitrogen" degradation; Fenton oxidation; Photocatalysis.

1 Introduction

Environmental remediation technologies are one of the most studied topics in environmental science because many industrial activities generate pollutants. The "three nitrogens" [ammonia nitrogen (NH_4^+-N), nitrate nitrogen (NO_3^--N) and nitrite nitrogen (NO_2^--N)] from industrial or domestic wastewater can lead to eutrophication of water bodies. The conversion of nitrogen to nitrate increases the nitrogen and oxygen demand (NOD), which can contribute to methemoglobinemia. High levels of nitrite in water increase the risk of cancer. Advanced oxidative processes involving photocatalytic mechanisms (photooxidation, photoreduction, and photodegradation) have received substantial attention in the past 50 years since the introduction of photocatalytic technology by Fujishima and Honda in 1970. Photocatalytic oxidation is an environmentally safe and promising method for degrading polluted wastewater (Chen et al. 2004;Lin et al. 2013). Compared with other techniques such as adsorption, chemical oxidation and ozonation, photocatalytic oxidation is a regenerative process with a lower cost. A photocatalyst with high activity is an important parameter in photocatalytic oxidation. TiO_2 is a well-known photocatalyst (J.Síma et al. 2013; K. Hashimoto et al.2013). However, the photocatalytic effect of pure TiO_2 is unsatisfactory, suggesting the need for modification of TiO_2 to improve its industrial application. In addition to doping and structural modification of TiO_2 nanoparticles to alter the photocatalytic properties, TiO2 supported on powdered activated carbon (PAC-TiO2), granular activated carbon (GAC-TiO2), and zeolite (Z-TiO2), i.e., supported TiO_2, also exhibits photocatalytic properties that differ from those of TiO_2 alone (Síma et al. 2013; Hashimoto et al. 2005; Harraz et al. 2013). SiO_2 aerogel is a very light solid with high porosity and remarkable thermal insulation (Rankin et al. 2014). It appears like a "foamy" translucent substance, hence the name "frozen smoke". Silica-titanium dioxide (SiO_2/TiO_2) composites are well-known materials (Camblor et al. 1995; Rao et al. 2003; Gao et al. 2012). Several studies have revealed the relationship between the photocatalytic activity of materials and the structure of surface TiO_2, method of preparation, and loading. In order to improve the stability and other properties of SiO_2/TiO_2, a synthetic method of SiO_2/TiO_2 has recently been developed, which involves the formation of hierarchical structures or aerogels. One-dimensional SiO_2-TiO_2 nanofibers exhibit large surface area and high thermal stability of anatase TiO_2, and SiO_2 effectively prevents phase transformation of TiO_2 from anatase to rutile structure at high temperatures (Cui et al. 2019; Wang et al. 2019). They exhibit strong ability to separate the photogenerated electron-hole pairs (Wang et al. 2019), resulting in improved photocatalytic performance. Therefore, SiO_2/TiO_2 aerogels exhibit excellent photocatalytic properties. Their mesoporous structure can overcome the inherent defects, especially in terms of electron transport. Results of a previous study confirmed the strong light-harvesting properties of SiO_2/TiO_2 with mesoporous structure (Kwon et al. 2015).

However, the Fe-CeO_x bimetallic compound supported by the surface of SiO_2/TiO_2 combines photocatalysis with Fenton degradation, resulting in enhanced degradation efficiency of target pollutants. According to Fenton's principle, hydroxyl radicals are generated by the decomposition of hydrogen peroxide (H_2O_2) in the presence of Fe^{2+}. Exposure to UV-Vis radiation improves the efficiency of this method, especially resulting in the regeneration of iron ions and OH• radicals, with increased specific surface area of TiO_2 boosting the activity of Fe-CeO_x bimetallic catalyst (Wang et al. 2011). A surface density of 2.5~14.5 CeO_x/nm^2 resulted in excellent catalytic activity.

In this study, TiO_2 nanoparticles were introduced into the catalyst system, and Fe-Ce bimetals were layered on the surface of SiO_2/TiO_2 to support bimetallic Fe-CeO_x to perform the photo-Fenton-catalyzed "trinitrogen" degradation. The effect of "trinitrogen" under different catalytic systems was explored. The degradation efficiency was determined and the possible mechanism was investigated.

2. Materials and methods

2.1 Materials

All chemicals were analytical, unpurified and used as received. Ethanol, tetrabutyl titanate, acetic acid, ferrous chloride tetrahydrate, cerium chloride heptahydrate, and hydrogen peroxide (AR) were purchased from Sinopharm Chemical Group,Shanghai,Chana.

2.2 Experimental procedures

2.2.1 Preparation of three catalysts including $SiO_2@TiO_2$-Fe-Ce

2.2.1.1 Preparation of $SiO_2@TiO_2$ composite aerogels

Preparation of SiO_2 aerogel sample was referenced to the invention patent we applied for, patent number: 202011361256.7. Then, a 3.3 mL aliquot of tetrabutyl titanate was added to 25 mL of absolute ethanol under magnetic stirring for 5 min. SiO_2 aerogel (0.8 g) was ultrasonically mixed with 75 mL of deionized water and stirred magnetically to form a suspension. The ethanol solution of tetrabutyl titanate was added dropwise into the suspension at a constant speed using a constant flow pump. The pH value of the system was controlled to approximately 2.3 by adding 0.5 mol/L acetic acid solution. The solution was suction-filtered after 1 h of reaction, and dried in an oven at 90°C for 6 h to obtain SiO_2@TiO_2 composite aerogels。

2.2.1.2 Preparation of three catalysts: SiO_2@TiO_2-Fe-Ce, SiO_2@TiO_2-Fe and SiO_2@TiO_2-Ce

SiO_2/TiO_2 composite aerogel prepared above was accurately weighed to 1.0 g and mixed with 50 mL of deionized water to form a suspension. Next, 2.24 g of $CeCl_3 \cdot 7H_2O$ and 2.39 g of $FeCl_2 \cdot 4H_2O$ were dissolved in 30 mL of deionized water and mixed uniformly at room temperature. The mixture was added to the suspension with a peristaltic pump at room temperature under a N_2 atmosphere, followed by the dropwise addition of 0.5 mol/L sodium hydroxide solution. Following suction filtration and washing three times with deionized water, the filtered product was placed in a vacuum-dried oven at 60°C for 6 h. The dried and filtered product was calcined at 500°C for 2 h to obtain SiO_2@TiO_2-Fe-Ce catalyst.

Further, only 2.39 g of $FeCl_2 \cdot 4H_2O$ was added during the preparation to obtain Fe-SiO_2@TiO_2 catalyst. However, the addition of 2.24 g$CeCl_3 \cdot 7H_2O$ yielded SiO_2@TiO_2-Ce catalyst.

2.2.2 Catalyst performance

A quartz reaction tube containing 30 mL each of ammonia nitrogen, nitrate nitrogen and nitrite nitrogen with a concentration of 0.1 mg/mL was treated with 0.01 g of catalyst, followed by static adsorption of the degradation solution for 20 min under dark to reach equilibrium. A small amount of the reaction solution was removed for centrifugation, and the absorbance of the supernatant (A_0) was determined. The UV light source in the UV reaction box was switched on for photocatalytic degradation. The solution was removed and centrifuged at high speed. The absorbance of the supernatant was denoted as At. The reaction time was 120 min. The degradation rate was calculated using the following formula:

$$H = (C_0 - C_t)/C_0 \times 100\% \qquad (2\text{-}1)$$

C_0 represents the concentration under adsorption equilibrium, whereas C_t is the concentration when the reaction time is t.

2.2.3 Effects of different conditions on the efficiency of three catalysts in Fenton degradation of "Trinitrogen"

A 250 mL conical flask containing 50 mL of 0.1 mg/mL ammonia nitrogen, nitrate nitrogen and nitrite nitrogen solutions was used. Two of the three conditions including pH, H_2O_2 dosage and catalyst system were fixed first, while changing the other condition. The conical flask was treated with different catalysts and shaken in a constant temperature oscillator. A sample was obtained every 20 min and its absorbance was measured. The degradation rate was then calculated.

2.2.4 Effects of different conditions on the photo-Fenton degradation efficiency of three nitrogen catalysts

A quartz UV reaction test tube containing 50 mL of 0.1 mg/mL ammonia nitrogen, nitrate nitrogen and nitrite nitrogen solutions was used to determine the effect of different conditions on the photo-Fenton degradation efficiency of the nitrogen catalysts. Two of the three conditions of pH, H_2O_2 dosage and catalyst system were held constant, and the third condition was changed. A 0.01 g of catalyst was added to the reaction test tube, and the reaction was carried out under a 300 W ultraviolet mercury lamp. A sample was obtained every 20 min to measure the absorbance and calculate the degradation rate.

3 Results and discussion

3.1 Characterization of catalyst

As shown in Figure 1(a), the diffraction peaks at 2θ of 25.68°, 37.6°, 48.2°, 55.4°, 57.2°, 64.6°, 69.4° and 75.1° correspond to eight crystal planes of anatase TiO_2 (101), (004), (200), (101), (211), (204), (220) and (215) (JCPDS, 21-1272), demonstrating that the TiO_2 in the catalyst material is anatase. No obvious diffraction peaks of Fe, Ce and SiO_2 are visible in the Figure, which may be due to the reduced levels of Fe and Ce in the catalyst, which led to weak diffraction peaks and absence of characteristic peaks of other phases, suggesting no new phase formation.

Figure 1(b) shows the N_2 adsorption and desorption curves of the catalyst and its pore size distribution. As shown in the Figure, the catalyst exhibits type IV adsorption and desorption curves, based on the IUPAC classification and a H3 hysteresis loop, indicating that the presence of mesoporous material with pore diameters ranging between 10 nm and 15 nm. According to the BET analysis, the $SiO_2@TiO_2$-Fe-Ce catalyst has a surface area of 455.8 m^2/g, a pore volume of 0,6025 cm^3/g, a most probable pore size of 16.23 nm, and an average pore size of 14.98 nm.

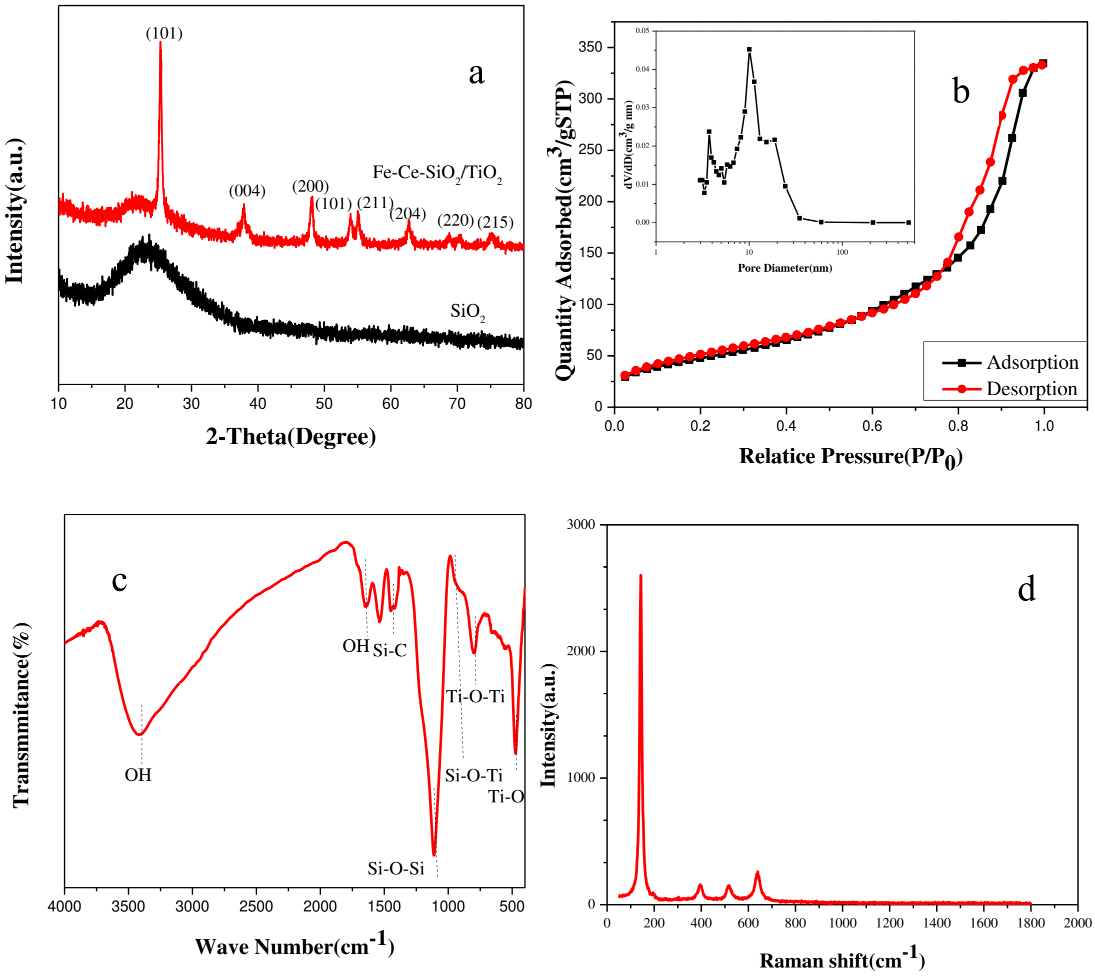

Fig.1 XRD, BET, FT-IR and Raman spectra of Fe-Ce-SiO_2/TiO_2 catalyst

Figure 1(c) shows the FT-IR spectrum of the $SiO_2@TiO_2$-Fe-Ce catalyst. As shown in the Figure, the broad bands of 3430 cm^{-1} and 1630 cm^{-1} in the spectrum correspond to the stretching of hydroxyl groups and surface adsorbed water, respectively. The samples exhibit characteristic peaks at 500 cm^{-1}, 1080 cm^{-1} and 950 cm^{-1}, which are attributed to the stretching vibrations of Ti-O and Si-O-Si of the silica framework, and Ti-O-Si, respectively. The hydroxyl and hydrogen bonds on the surface of the aerogel enhance its adsorption capacity for "trinitrogen" and therefore promote subsequent photocatalytic degradation. These results suggest that the incorporation of TiO_2 into SiO_2 results in the formation of a binary TiO_2-SiO_2 system, and the vibrational peaks indicate the interaction between Ti and Si at the molecular level.

In order to validate the presence of TiO_2 in the $SiO_2@TiO_2$-Fe-Ce catalyst, the sample was characterized by Raman spectroscopy. The results presented in Figure 1(d) indicate that 198(Eg), 398(Eg), 515(Eg) and 640(Eg), correspond to anatase TiO_2, which are consistent with the results of XRD analysis.

3.2 XPS Analysis

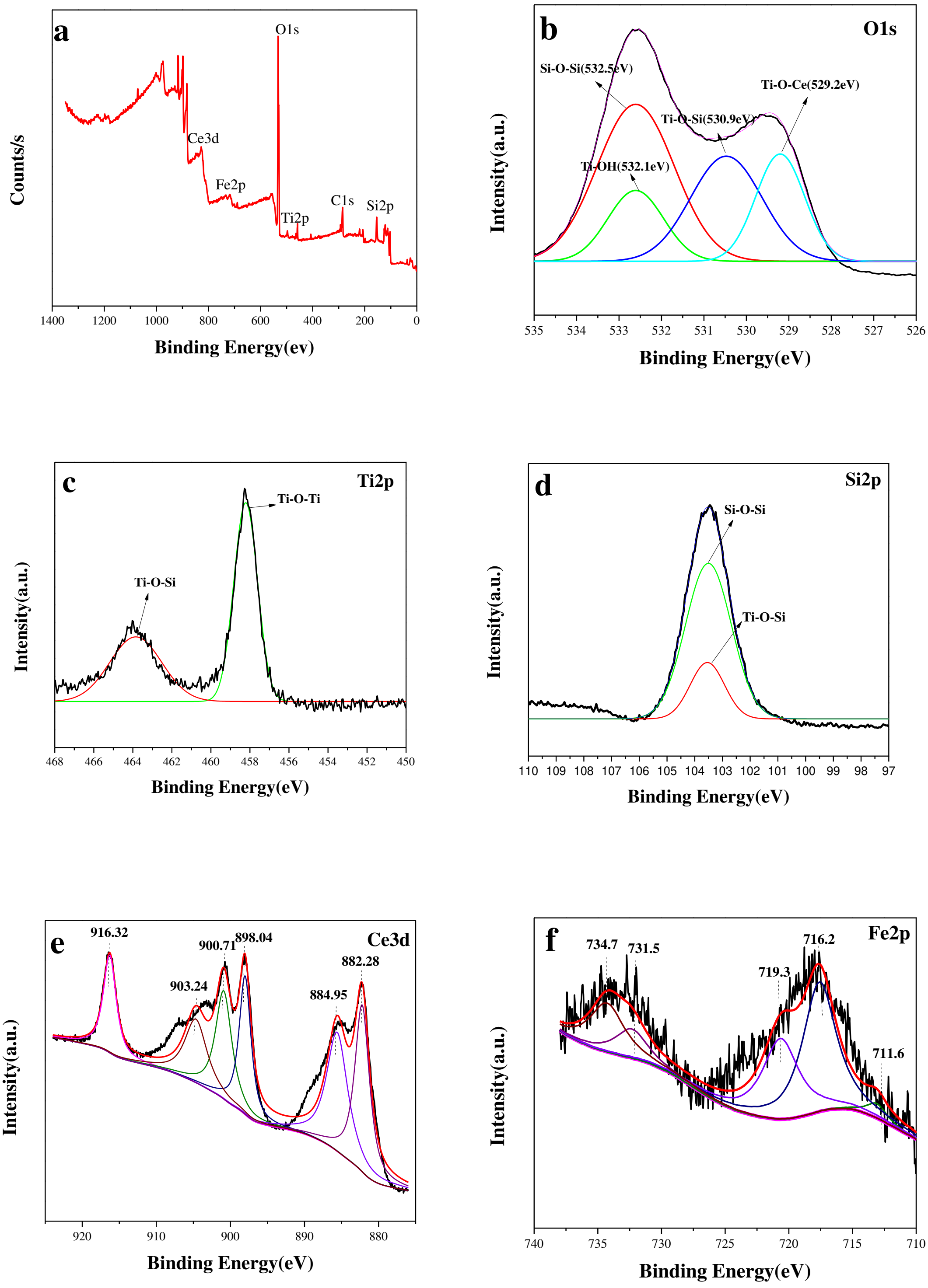

Fig. 2 XPS of SiO_2@TiO_2-Fe-Cecatalyst

Figure 2 illustrates the XPS characterization of the SiO_2@TiO_2-Fe-Ce catalyst. The elemental composition and chemical valence states of elements, such as O, Si, Ti, Ce, and Fe on the surface of the catalyst samples were studied. Figure 2(a) represents the full spectrum of the catalyst sample, indicating the presence of six main elements, including C, Si, O, Fe, Ce and Ti. The C element may be due to incomplete calcination or contaminant residues on the sample surface. Figures 2(b) to 2(f) represent the high-resolution spectra of O1s, Ti2p, Si2p, Ce3d and Fe2p, respectively. As shown in Figure 2(b), the O element exhibits four chemical forms in the catalyst, with electron binding energies of 529.2 eV, 530.9 eV, 532.1 eV and 532.5 eV attributed to Ti-O-Ce and Ti-O-Si, Ti-OH and Si-O-Si chemical bonds, respectively. Figure 2(c) is the XPS high-resolution spectrum of Ti2p showing two chemical states of Ti in the catalyst system. The peak of the electron binding energy is attributed to Ti^{4+} in the catalyst, which corresponds to the binding energy of Ti in Ti-O-Ti and Ti-O-Si. Figure 2(d) represents the XPS image of Si2p, with the two peaks appearing at 102.6 eV and 103.2 eV, respectively, after the peak separation, which are attributed to Si2p in Si-O-Si and Ti-O-Si. As shown in Figure 2(e), the results of peak separation of Ce3d reveal the characteristic peaks of electron binding energy at 882.28 eV, 884.95 eV and 898.04 eV belonging to the spin-orbits of the electronic states of Ce3d5/2, while the peaks at 900.71 eV, 903.24 eV and the characteristic peak at 916.32 eV are assigned to the spin-orbit of the electronic state of Ce3d3/2. The characteristic peaks of binding energy at 884.95 and 903.24 eV correspond to Ce^{3+} (3d104f1 electronic state), and the rest of the characteristic peaks are assigned to Ce^{4+} (3d104f0 electronic state) (Shao et al. 2013), indicating that both Ce^{3+} and Ce^{4+} exist on the catalyst surface. The presence of oxygen vacancies and unsaturated bonds in Ce^{3+} increases the chemical adsorption of oxygen on the surface of the Fe-Ce-SiO_2/TiO_2 catalyst. Ce^{4+} captures the photogenerated electrons to generate Ce^{3+}. The photogenerated electrons are transferred to the O_2 molecules adsorbed on the surface of the catalyst. Finally, superoxide radicals ($O_2\cdot$) are generated, which increase the photocatalytic efficiency of the catalyst. Figure 2(f) is the XPS spectrum of Fe2p indicating that the characteristic peak at 711.6 eV belongs to Fe2+ while the characteristic peaks at 716.2 eV and 719.3 eV belong to Fe^{3+} (Lenza et al. 2002; Vilarrasa et al.2015), indicating the presence of Fe on the catalyst surface in two forms, Fe^{2+} and Fe^{3+}.

3.3 TEM and SEM characterization

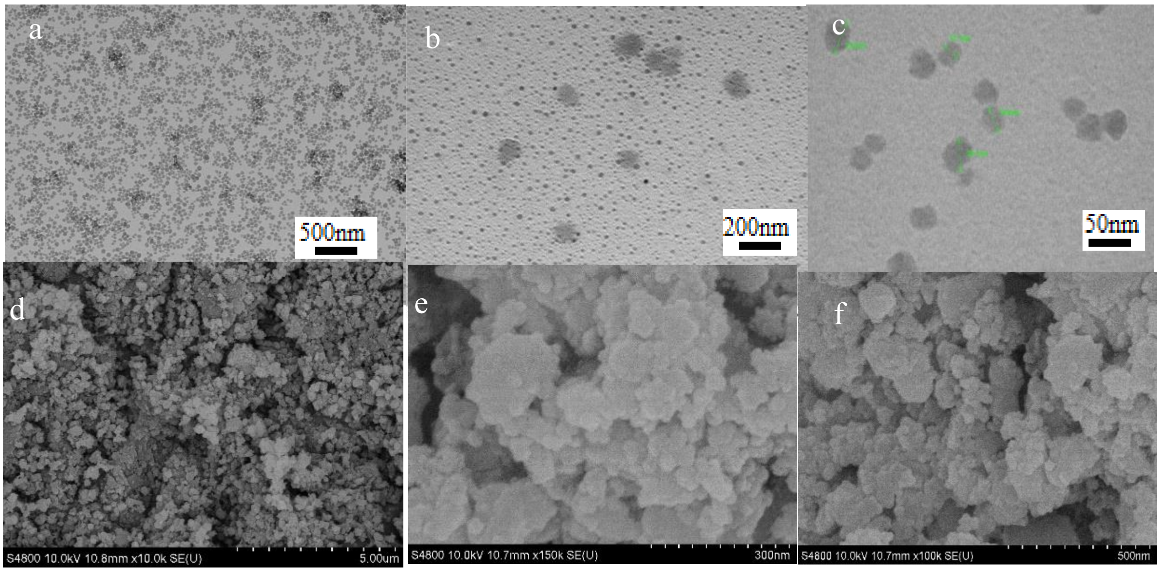

Fig. 3 TEM and SEM images of SiO_2@TiO_2-Fe-Ce catalyst

Figures 3 a, b, and c represent the TEM images of the SiO_2@TiO_2-Fe-Ce catalyst under different magnifications. The catalyst samples obtained after Fe and Ce doping exhibit strong dispersion and uniform particle size. As shown in Figure 3(c), the average diameter is about 15 nm.

Figures 3 d, e, and f are the SEM images of the SiO_2@TiO_2-Fe-Ce catalyst under different magnifications, revealing a spherical catalyst structure and uniform distribution, with typical SiO_2 gas condensation. The microstructure is similar to that of glue, with uniform pore distribution and particle aggregation after the introduction of TiO_2. As shown in the Figure, the anatase-type TiO_2 particles are mainly located on the surface of spherical particles, and doping with iron and cerium yields strong photocatalytic activity.

3.4 **Effect of pH on the degradation of "trinitrogen" by SiO_2@TiO_2-Fe-Ce catalyst with or without photocatalysis**

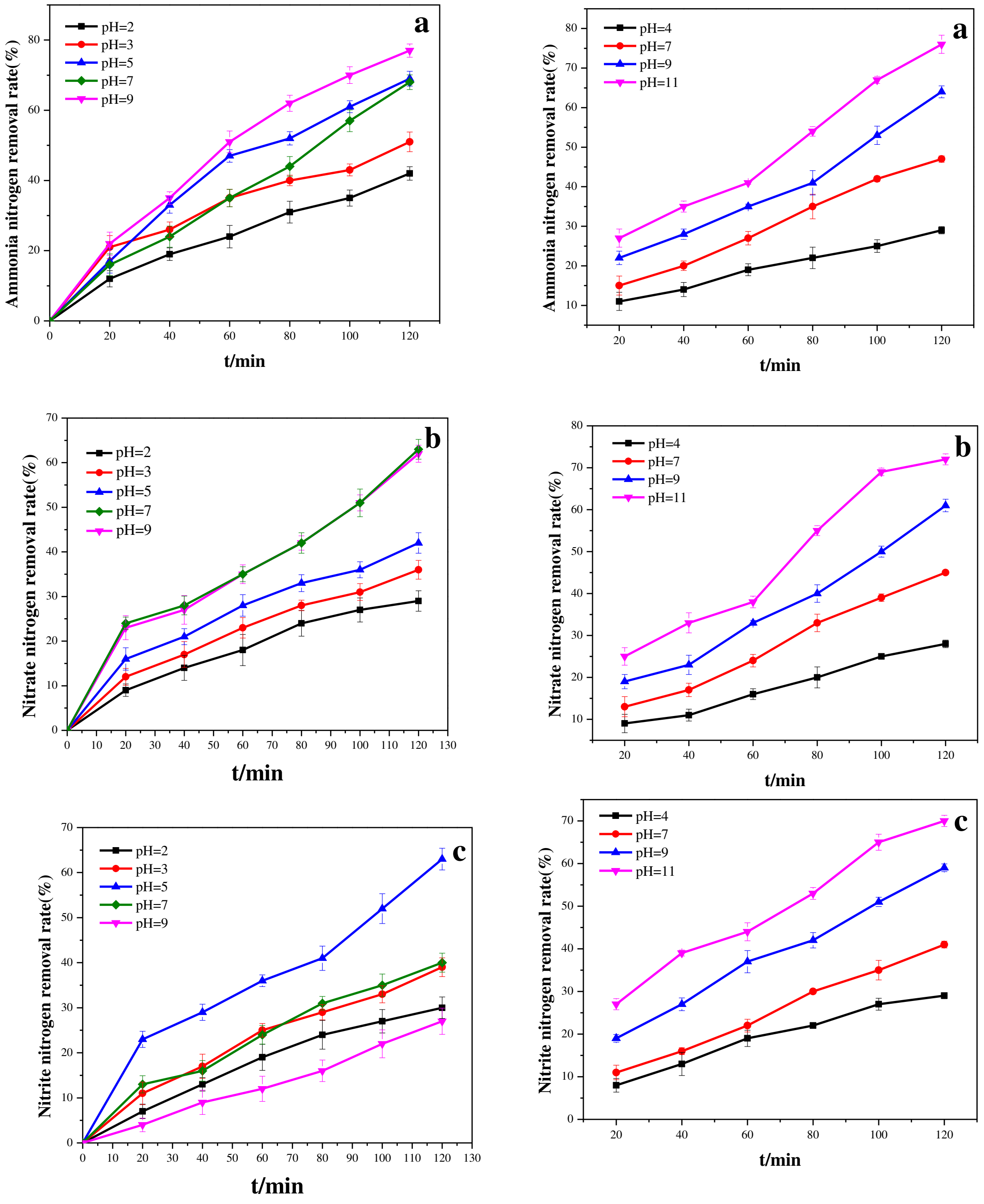

$[H_2O_2]$ = 20 mmol/L; iron-cerium molar ratio, 1:1; reaction time, 120 min

Fig. 4 Degradation rate of "three nitrogens" by catalysts under different pH conditions: (a) ammonia nitrogen, (b) nitrate nitrogen, (c) nitrite nitrogen

$H_2O_2+Fe^{2+}\rightarrow Fe^{3+}+OH^{-}+OH\cdot$ (3-1) $Ce^{4+}+e^{-}\rightarrow Ce^{3+}$ (3-6)

$HO\cdot+Fe^{2+}\rightarrow Fe^{3+}+HO^{-}$ (3-2) $Fe^{2+}+Ce^{4+}\rightarrow Ce^{3+}+Fe^{3+}$ (3-7)

$Fe^{3+}+H_2O_2 \rightarrow Fe\text{-}OOH_2+H^+$ (3-3) $Ce^{3+}+HO\cdot \rightarrow Ce^{4+}+OH^-$ (3-8)

$Fe\text{-}OOH^{2+} \rightarrow Fe^{2+}+HO_2\cdot$ (3-4) $Ce^{3+}+HO_2/O_2^{-}\cdot \rightarrow Ce^{4+}+H_2O$ (3-9)

$Fe^{3+}+HO_2\cdot \rightarrow Fe^{2+}+O_2+H^+$ (3-5) $Ce^{4+}+H_2O_2 \rightarrow HO_2\cdot/O_2^{-}\cdot+H^+$ (3-10)

$Ce^{4+}+HO_2\cdot/O_2^{-}\cdot \rightarrow Ce^{3+}+H^++O_2$ (3-11)

Ce^{4+} cannot be produced when the pH of the system is less than 4.0, and its removal cannot be enhanced. Increase in pH to 5.0 generates intermediates of $Ce(OH)_3OOH$ in the system, which promote the conversion of Ce^{3+} to Ce^{4+} as well as the generation of $HO_2\cdot/O_2$-·, facilitating the conversion of Fe^{3+} to Fe^{2+}, thereby generating additional HO· and improving the reaction performance. Figure 4.8(b) shows the same trend as Figure 4.7(a), with a degradation efficiency of 63.4% without significant difference at pH 7.0 and 9.0. Figure 4(c) shows the degradation of nitrite nitrogen, with the highest degradation efficiency of 64.2% at pH 5.0.

Figures 4 (d) (e) and (f) show the degradation efficiency of SiO_2@TiO_2-Fe-Ce catalyst for "trinitrogen" under different pH values, indicating that the increase of system pH enhances degradation rate of "three nitrogens". The degradation efficiency was the best at pH 11. The removal rate of ammonia nitrogen reached 75.9%, while the removal efficiency of nitrate nitrogen reached 71.3%, and the removal efficiency of nitrite nitrogen reached 71.3%. The rate of 70.1% may be explained by the effect of initial pH of the system on the presence of "trinitrogen" in the solution. A gradual increase in the pH increases the number of OH^- ions in the system generated by photo-Fenton catalysis. The increase of OH· in the presence of ammonia nitrogen generates further free NH3 in the solution. The rare earth element Ce generates electrons and holes due to its unique outer electronic structure. In addition, Ce also carries a specific oxygen storage capacity. It can increase the charge generated on the surface of the SiO_2@TiO_2-Fe-Ce catalyst, which is conducive to the transfer of holes from the interior of the particles to the surface for "trinitrogen" adsorption. A large amount of OH- on the entire interface is also conducive to OH · generation. Further, as the reduced steric hindrance of the free "trinitrogen" facilitates the catalytic reaction while Fe is a better hole-trapping agent with a strong synergistic effect when combined with Ce, which greatly increases the overall catalytic activity. The removal efficiency of the "three nitrogens" is also increased. The relevant reactions are represented by equations (3-12) to (3-19):

$$SiO_2@TiO_2\text{-}Fe\text{-}Ce+h\nu \rightarrow SiO_2@TiO_2\text{-}Fe\text{-}Ce+(e^-+h^+) \quad (3\text{-}12)$$

$$Ce^{4+}+e^- \rightarrow Ce^{3+} \quad (3\text{-}13)$$

$$Fe^{3+}+e^- \rightarrow Fe^{2+} \quad (3\text{-}14)$$

$$Ce^{3+} + O_2 \rightarrow Ce^{4+} + \cdot O_2^- \tag{3-15}$$

$$Fe^{2+} + O_2 \rightarrow Fe^{3+} + \cdot O_2^- \tag{3-16}$$

$$H_2O + h^+ \rightarrow H^+ + \cdot OH \tag{3-17}$$

$$\cdot O_2^- + 2H^+ \rightarrow 2\cdot OH \tag{3-18}$$

$$Dye^+ + \cdot HO \rightarrow \text{degradation products} \tag{3-19}$$

3.5 Effect of H_2O_2 dosing concentration on photocatalytic degradation rate of "trinitrogen"

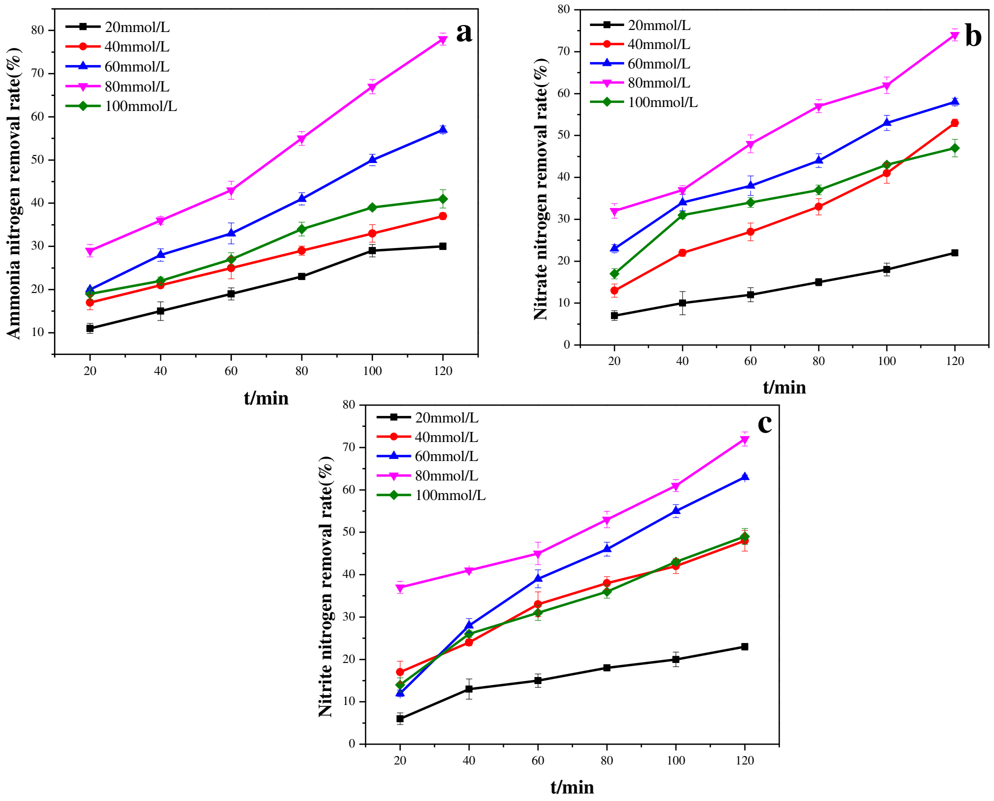

Fig. 5 The degradation rate of the "three nitrogen" by catalysts under different H_2O_2 dosing concentrations. (a) ammonia nitrogen, (b) nitrate nitrogen, (c) nitrite nitrogen

It can be seen from Figure 5 that under similar experimental conditions, the increases H_2O_2 dosage increases the rate of photocatalytic degradation of "trinitrogen" initially, followed by a decline. When the dosage of H_2O_2 was 80 mmol/L the degradation efficiency of the catalysts for "three nitrogens" reached the highest level, with a 79.8% degradation rate for ammonia nitrogen, whereas the degradation rate of nitrate nitrogen was 74.6%, and the degradation rate of nitrite nitrogen was 73.7%. H_2O_2 itself captures the photogenerated electrons. The addition of Fe prolongs the recombination of holes and electrons. The doping of rare earth Ce results in additional photogeneration of electrons by the holes. In the case of UV light irradiation, H_2O_2 itself decomposes to generate adequate OH·, suggesting that Fe-Ce-SiO_2/TiO_2 catalyst and H_2O_2 exhibit a strong synergistic effect under UV light. Excessive concentrations of H_2O_2 have a negative effect on the overall catalysis probably because the high levels of H_2O_2 and self-clearance contribute to the reduction of OH· and attenuation of the "trinitrogen" degradation.

3.6 Degradation rate of "trinitrogen" under different catalytic systems

3.6.1 Effects of different catalytic systems on the degradation rate of ammonia nitrogen

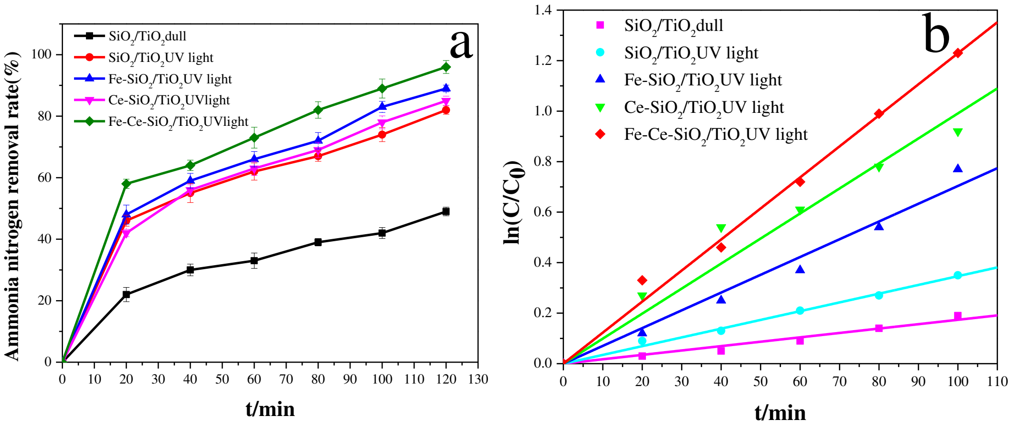

Figure 6 Photocatalytic degradation of ammonia nitrogen. Pseudo-first-order kinetic equation of photocatalytic degradation of ammonia nitrogen

Figure 6a shows the degradation rate of ammonia nitrogen by sample SiO_2/TiO_2 under dark conditions and the degradation rate curves of SiO_2/TiO_2, Fe-SiO_2/TiO_2, Ce-SiO_2/TiO_2 and Fe-Ce-SiO_2/TiO_2 under UV light. As shown in the Figure, the efficiency of catalytic degradation of ammonia nitrogen under UV light is greatly improved compared with dark conditions. Compared with Fe-SiO_2/TiO_2 and Ce-SiO_2/TiO_2, the ammonia nitrogen degradation rate of TiO_2 samples and Fe-Cerium co-doped samples is always higher than that of single dopants. The degradation rate of ammonia nitrogen reached 88.7% within 120 min, which was 10%-20 higher than under other conditions, indicating that the photocatalytic performance of the catalyst was significantly improved after doping with iron and cerium. The improved performance of the catalyst after iron-cerium bimetallic doping may be due to the formation of Ti-O-Si bonds after TiO_2 was added to the system, indicating the formation of additional defects and electron capture, which further inhibited the agglomeration of nanoparticles in the system. Ce^{4+} in the form of Ce^{3+}/Ce^{4+} ion pair captures photogenerated electrons as a

Lewis acid, which facilitated the separation of electron-hole pairs.

Table 1 Kinetic equation of ammonia nitrogen solution degradation with different catalysts

Sample/Condition	First order kinetic equation	R^2	$K(min^{-1})$
SiO_2/TiO_2 dull	y =0.00205x-0.023	0.96977	0.00205
SiO_2/TiO_2 UV light	y =0.0033x+0.012	0.98667	0.0033
Fe-SiO_2/TiO_2 UV light	y =0.00795x-0.067	0.97419	0.00795
Ce-SiO_2/TiO_2 UV light	y =0.0077x+0.162	0.95987	0.0077
Fe-Ce-SiO_2/TiO_2 UV light	y =0.01165x+0.047	0.98439	0.01165

Figure 6b represents the kinetic reaction equation of different catalysts using UV light as the light source. The change in ammonia nitrogen concentration curve under different reaction times fitted the kinetic curve, based on the kinetic equation under different series. The catalytic degradation of ammonia nitrogen conforms to first-order kinetic equation. The fitting parameters of the first-order kinetic equation are shown in Table 1. The relatively high linear correlation suggests increased catalytic degradation of ammonia nitrogen in dilute solution. The photocatalytic degradation reaction basically follows the first-order kinetic equation.

3.6.2 Effects of different catalytic systems on nitrate nitrogen degradation rate

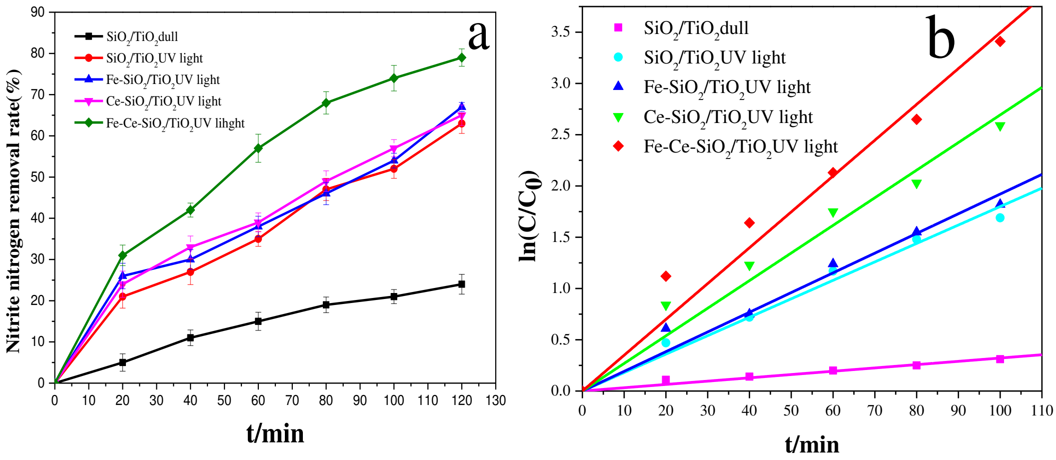

Figure 7 (a) Photocatalytic degradation of nitrate nitrogen. (b) Pseudo-first-order kinetic equation of photocatalytic degradation of nitrate nitrogen

Table 2 Kinetic equations for catalytic degradation of nitrate nitrogen solution

Sample/Condition	First order kinetic equation	R^2	$K(min^{-1})$
SiO_2/TiO_2dull	y =0.0029x+0.0233	0.97069	0.0029

SiO_2/TiO_2 UV light	y =0.0017x+0.0695	0.9805	0.0017
Fe-SiO_2/TiO_2 UV light	y =0.0177x+0.1085	0.97395	0.0177
Ce-SiO_2/TiO_2 UV light	y =0.0243x+0.1895	0.9735	0.0243
Fe-Ce-SiO_2/TiO_2 UV light	y =0.0316x+0.2442	0.9736	0.0316

Figure 7b represents the kinetic reaction equation of different catalysts using UV light. The change in the nitrate nitrogen concentration under different reaction times is subjected to kinetic curve fitting. The fitting kinetic equation under different series suggests that the catalytic degradation of nitrate nitrogen conforms to first-order reaction kinetics, and the fitting parameters of the first-order kinetic equation are shown in Table 2. The high linear correlation suggests that the photocatalytic degradation of nitrate nitrogen in dilute solution follows the first-order kinetics.

3.6.3 Effects of different catalytic systems on nitrite nitrogen degradation rate

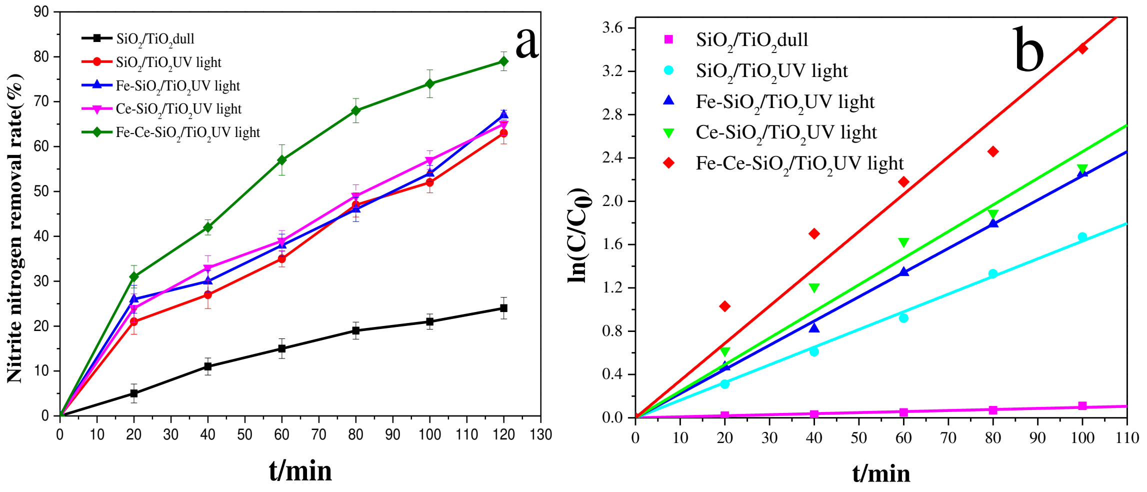

Figure 8(a) Photocatalytic degradation of nitrite nitrogen; (b) pseudo-first-order kinetic equation representing photocatalytic degradation of nitrite nitrogen

Figure 8(a) shows the degradation rate of nitrite nitrogen under different catalytic systems. As shown in the Figure, the catalytic degradation rate of nitrite nitrogen under UV light is significantly higher than that under dark conditions, indicating that the photo-Fenton-catalyzed degradation effectively improves the degradation efficiency of nitrite nitrogen. The degradation efficiency of bimetallic doping was higher than that of single metal, reaching 80.2% within 120 min, indicating a synergistic effect of iron-cerium bimetallic combination.

Table 3 Kinetic equations of degradation of nitrite nitrogen solution by different catalysts

Sample/Condition	First order kinetic equation	R^2	K(min^{-1})
SiO_2/TiO_2dull	y =0.00103x-0.00476	0.94704	0.00103
SiO_2/TiO_2 UV light	y =0.01674x-0.03048	0.99627	0.01674
Fe-SiO_2/TiO_2 UV light	y =0.02254x-0.01381	0.9978	0.02254
Ce-SiO_2/TiO_2 UV light	y =0.02257x-0.01289	0.97349	0.02257
Fe-Ce-SiO_2/TiO_2 UV light	y =0.03117x+0.2381	0.96199	0.03117

As shown in Figure 8(b) and Table 3, the photo-Fenton-catalyzed degradation of nitrite nitrogen by Fe-Ce-SiO_2/TiO_2 catalyst conforms to the first-order reaction kinetics, and its linear relationship is represented by the equation, y = 0.03117x + 0.2381, R^2= 0.96199.

3.7 Catalytic degradation products and possible mechanisms

Figure 9(a) shows the levels of various components of the degradation products following 6 sessions of photocatalysis of ammonia nitrogen simulating wastewater

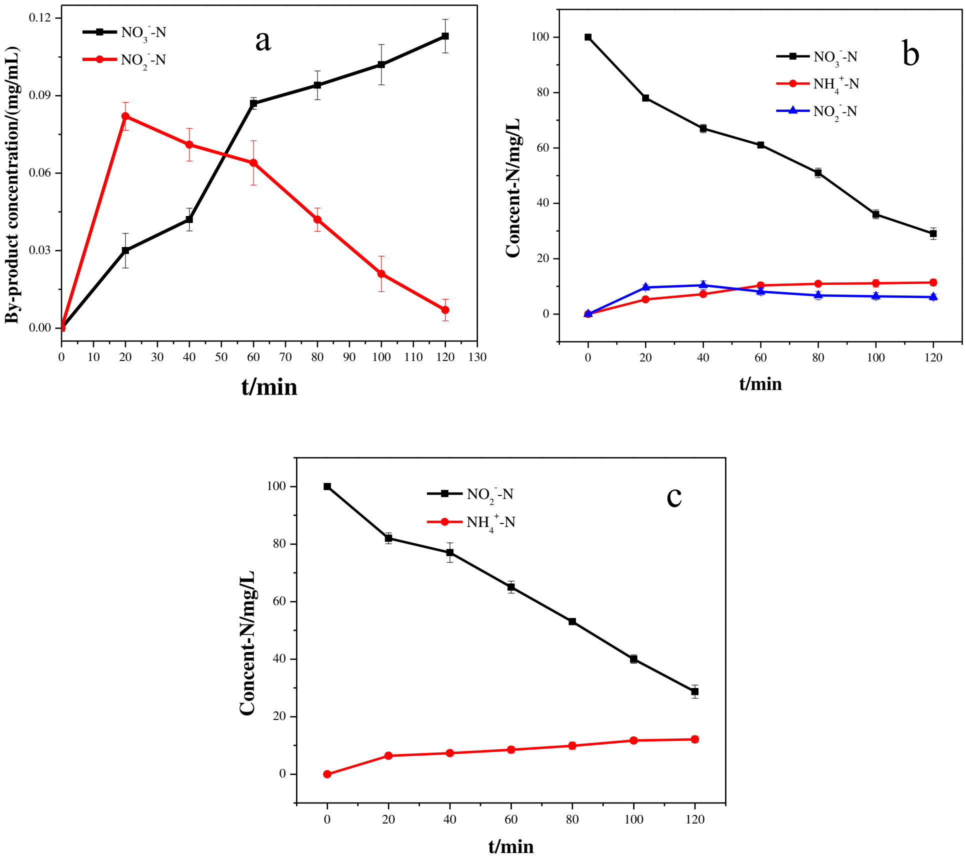

Fig.9 Graphical representation of temporal variation in the levels of ammonia nitrogen (a),

nitrate nitrogen (b) and nitrite nitrogen (c) degradation products

As shown in Figure 9(a), the final levels of nitrate nitrogen and nitrite nitrogen in 1 mg/mL of ammonia nitrogen degradation products were 0.114 mg/mL and 0.012 mg/mL, respectively, while the degradation rate of ammonia nitrogen under this condition was 88.7%, suggesting that nearly 62.08% of ammonia nitrogen was finally converted to N_2 in the whole reaction. Kishor (Kishor et al. 2015)proposed that strong oxidizing free radicals and superoxide ions are generated during ammonia nitrogen degradation by this series of catalysts, which induces a series of redox reactions summarized by the reaction equations (3-20) to (3- 24):

$$NH_4^+ + 2OH^- \rightarrow NO_2^- + 3H_2 \tag{3-20}$$

$$2NO_2^- + O_2 \rightarrow 2NO_3^- \tag{3-21}$$

$$NO_3^- + 2H^+ + 2e^- \rightarrow NO_2^- + H_2O \tag{3-22}$$

$$NO_3^- + 10H^+ + 8e- \rightarrow NH_4^+ + 3H_2O \tag{3-23}$$

$$2NO_3^- + 12H^+ + 10e^- \rightarrow 2N_2 + 3H_2O \tag{3-24}$$

The above equations indicate that specific intermediates are generated during ammonia nitrogen degradation, and approximately 62.08% of ammonia nitrogen may eventually be converted to N_2.

As shown in Figure 9(b), the degradation rate of nitrate nitrogen gradually increased at the beginning of the reaction, reaching 71.1% at 120 min. The degradation of nitrate nitrogen gradually increased the levels of nitrite nitrogen and ammonia nitrogen in the system. The nitrite nitrogen content reached the maximum within 40 min, followed by a decline eventually, while the ammonia nitrogen content increased and plateaued, indicating that nitrite nitrogen was an intermediate, and its degradation mechanism is shown in Figure 10 (a).

As shown in Figure 9(c), the final degradation product of nitrite nitrogen was ammonia nitrogen, with a degradation efficiency reaching 71.4% within 120 min, and the final ammonia nitrogen concentration was 12.3 mg/L, indicating the presence of gaseous products during the degradation. The formation of NO_2^- may involve N_2, NO, N_2O and other nitrogen oxides, and the overall gaseous product conversion efficiency was calculated to be 38.12%, indicating that the photocatalytic degradation of NO_2^- entailed oxidation and reduction (Ebrahimi et al. 2017). The primary oxide species carry photogenerated holes (h^+), superoxide (O_2-) and hydroxyl radicals (.OH) during heterogeneous photocatalytic degradation(Tomova et al. 2015). Figure 10(b) shows the possible degradation mechanism.

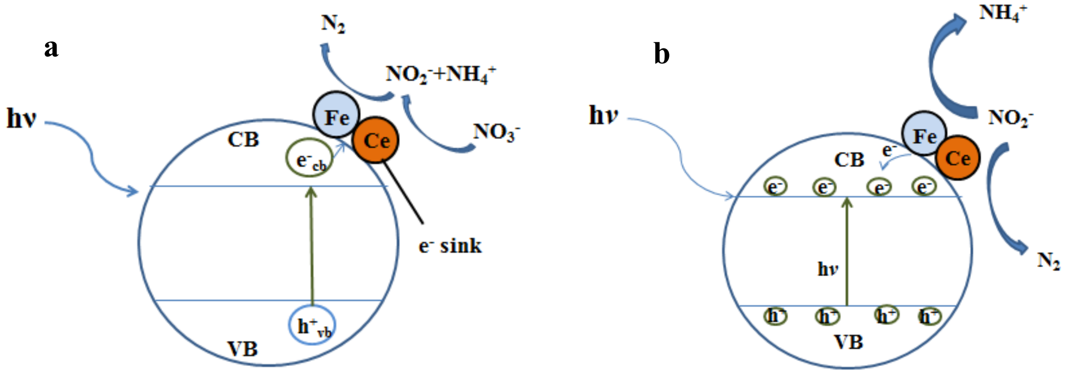

Fig.10 (a) Possible mechanism of photocatalytic degradation of nitrate nitrogen; (b) Possible mechanism of photocatalytic degradation of nitrite nitrogen

Figure 10(a) shows the possible mechanism of photocatalytic degradation of nitrate nitrogen, suggesting that N_2 and ammonia nitrogen are the final degradation products. The first step of nitrate photolysis involves the transition of $\pi \rightarrow \pi^*$ in the excited state. The unstable nitrate species is produced as shown in equation (3-26). The $NO_2\cdot$ preferentially dimerizes and releases N_2O_4, followed by rapid hydrolysis and subsequent generation of NO_2^-, which is reduced to NH^{4+} and N_2(Sowmya et al. 2014; Dong et al. 2019). The related reaction equations are as follows:

$$H_2O+h_{vb}^+ \rightarrow H^+ + OH\cdot \quad (3\text{-}25)$$

$$NO_3^- + h\nu \rightarrow [NO_3^-]^* \rightarrow NO_2^- + 1/2O_2 \rightarrow NO_2\cdot + O^-\cdot \quad (3\text{-}26)$$

$$O^-\cdot + H_2O \leftrightharpoons OH\cdot + OH^- \quad (3\text{-}27)$$

$$OH\cdot + \text{degradants} \rightarrow \text{products} \quad (3\text{-}28)$$

$$2NO_2\cdot \leftrightharpoons N_2O_4 \quad (3\text{-}29)$$

$$N_2O_4 + H_2O \rightarrow NO_3^- + NO_2^- + 2H^+ \quad (3\text{-}30)$$

$$NO_3^- + e^- \rightarrow NO_3^{2-} \quad (3\text{-}31)$$

$$NO_3^{2-} + H_2O \rightarrow NO_2\cdot + 2OH^- \quad (3\text{-}32)$$

$$NO_2\cdot + e^- \rightarrow NO_2^- \quad (3\text{-}33)$$

$$NO_2^- + 8H^+ + 6e^- \rightarrow NH_4^+ + 2H_2O \quad (3\text{-}34)$$

$$2NO_2^- + 8H^+ + 6e^- \rightarrow N_2 + 4H_2O \quad (3\text{-}35)$$

4 Conclusion

In this study, Fe-Ce-SiO_2/TiO_2 catalyst was fabricated by introducing TiO_2 into the catalytic system and using tetrabutyl titanate as the precursor via impregnation. The catalyst was characterized by XRD, FT-IR, BET, TEM, SEM, XPS and other methods. The results show that TiO_2 in the catalyst exists in the form of anatase on the surface, and the prepared catalyst carries a high specific surface area (455.8 m^2/g) and pore volume (0.6025 cm^3/g). The catalyst exhibits high dispersibility, and the iron and cerium elements in the system exist in the form of Fe^{2+}/Fe^{3+} and Ce^{3+}/Ce^{4+}.

In addition, the photo-Fenton degradation performance of “trinitrogen” in the catalyst was studied. The results showed optimal photocatalytic effect of Fenton's reagent at a catalyst dosage of 0.01 g, pH 11.0, and H_2O_2 concentration of 80 mmol/L. The degradation efficiency of "trinitrogen" remained above 70%. The photo-Fenton degradation of "trinitrogen" under different catalytic systems conformed to first-order reaction kinetics. The corresponding degradation products of "trinitrogen" were analyzed.

Authors Contributions

Jie Li: Methodology，Investigation.

Yuxiang Yang: Conceptualization， Supervision, Writing-Original Draft, Project administration，Funding acquisition, Writing and Editing.

Yan Huang: Formal analysis, Visualization.

Hongming Yuan: Validation,Resources.

Zhiyong Han: Data Curation.

Chaoying Ni: Reviewing.

Funding Information: This work was supported by the National Natural Science Foundation of China (20577010, 20971043), the Fundamental Research Funds for the Central Universities,and the Open Project Program of State Key Laboratory of Inorganic Synthesis and Preparative Chemistry, Jilin University.

Data availability: The datasets used and/or analyzed during the current study are available from the corresponding author on reasonable request.

Declarations

Ethics approval and consent to participate: Not applicable.

Consent for publication: Not applicable.

Competing interests: The authors declare no competing interests

References

Cui L, Song Y, Wang F, Sheng Y, Zou H (2019)Electrospinning synthesis of SiO_2-TiO_2 hybrid nanofibers with large surface area and excellent photocatalytic activity, Applied Surface Science,488:284–292.

Camblor M.A., Constantini M., Corma A.,Esteve P., Gilbert L., Martinez A., et al.(1995)A new highly efficient method for the synthesis of Ti-Beta zeolite oxidation catalyst. Applied Catalysis A: General,133:0–4.

Chen Y., Wang K., Lou L. (2004)Photodegradation of dye pollutants on silica gel supported TiO_2 particles under visible light irradiation. Journal of Photochemistry and Photobiology A: Chemistry,63:281–287.

Dong C,Huang C, Nguyena Thanh-Binh, Hsiung Ching-Feng, Wu Chung-Hsin, Lin Yi-Li, Chen Chiu-Wen, Hung Chang-Mao (2019)The degradation of phthalate esters in marine sediments by persulfate over iron–cerium oxide catalyst. Science of the Total Environment, 696:133973-133982.

Ebrahimi-Gatkash Mehdi, Younesi Habibollah, Shahbazi Afsaneh, Heidari Ava (2017)Amino-functionalized mesoporous MCM-41 silica as an efficient adsorbent for water treatment: batch and fixed-bed column adsorption of the nitrate anion. Applied Water Science,7:1887–1901.

Gao X.-D., Li X.-M., Gan X.-Y., Wu Y.-Q., Zheng R.-K., Wang C.-L., et al.(2012)Aerogel based SiO_2–TiO_2 hybrid photoanodes for enhanced light harvesting in dye-sensitized solar cells. Journal of Materials Chemistry,22:18930.

Harraz F.A., Abdel-Salam O.E., Mostafa A.A., Mohamed R.M., Hanafy M. (2013)Rapid synthesis of titaniasilica nanoparticles photocatalyst by a modified sol–gel method for cyanide degradation and heavy metals removal.Journal of Alloys and Compounds ,551:1–7.

Hashimoto K., Irie H., Fujishima A. (2005)TiO_2 photocatalysis: a historical overview and future prospects. Japanese Journal of Applied Physics,44:8269–8285.

Kwon DW, Hong SC (2015)Correlation between Physicochemical Properties of Various Commercial TiO_2 Supports and NH_3-SCR Activities of Ce/Ti Catalysts, Appl. Chem. Eng., Vol. 26, No. 2, 193-198

Kishor Rupak,Aloke Kumar Ghoshal(2015)APTES grafted ordered mesoporous silica KIT-6 for CO_2 adsorption. Chemical Engineering Journal,262: 882-890.

Lin L., Chai Y., Zhao B., Wei W., He D., He B., et al.(2013)Photocatalytic oxidation for degradation of VOCs. Inorganic Chemistry Communications, 3:14–25.

Lenza R.F.S., Vasconcelos W.L. (2002)Synthesis of titania-silica materials by sol-gel. Materials Research Letters,5:497–502.

Rankin J.M., Baker S., Klabunde K.J. (2014)Mesoporous aerogel titanium oxidesilicon oxide combinations as adsorbents for an azo-dye.Microporous and Mesoporous Materials, 190:105–108.

Rao A.V., Kulkarni M.M., Pajonk G.M., Amalnerkar D.P., and Seth T. (2003)Synthesis andcharacterization of hydrophobic silica aerogels using trimethylethoxysilane as a co-precursor.Journal of Sol-Gel Science and Technology,27(2): 103–109.

Sowmya A,Meenakshi S,(2014)A novel quaternized resin with acrylonitrile/divinylbenzene/ vinylbenzyl chloride skeleton for the removal of nitrate and phosphate.Chemical Engineering Journal,257:45–55.

Shao G.N., Kim Y., Imran S.M., Jeon S.J., Sarawade P.B., Hilonga A., et al.(2013)Enhancement of porosity of sodium silicate and titanium oxychloride based TiO_2-SiO_2 systems synthesized by sol-gel process and their photocatalytic activity,.Microporous and Mesoporous Materials, 179: 111–121.

Síma J., Hasal P. (2013)Photocatalytic degradation of textile dyes in a TiO_2/UV system. Transactions of the Institution of Chemical Engineers,32:79–84.

Tomova D.,Iliev V.,Eliyas A.,et al(2015)Promoting the oxidative removal rate of oxalic acid on gold-doped CeO_2/TiO_2 photocatalysts under UV and visible light irradiation. Separation and purification Technology,156:715-723.

Vilarrasa-Garcia E,Ortigosa E.M., Moya,J.A. Cecilia,C.L. Cavalcante,J. Jiménez-Jiménez,D.C.S. Azevedo,E. Rodríguez-Castellón(2015)CO_2 adsorption on amine modified mesoporous silicas: Effect of the progressive disorder of the honeycomb arrangement.Microporous and Mesoporous Materials,209:172-183.

Wang H.L., Liang W.Z., Jiang W.F. (2011)Solar photocatalytic degradation of 2-sec-butyl-4,6-dinitrophenol (DNBP) using TiO_2/SiO_2aerogel composite photocatalysts. Materials Chemistry and Physics, 130: 1372–1379.

Wang W, Chen H, Fang J, Lai M (2019)Large-scale preparation of rice-husk-derived mesoporous SiO_2@TiO_2 as efficient and promising photocatalysts for organic contaminants degradation, Applied Surface Science ,467–468 :1187–1194.